Stripeless incommensurate magnetism in strongly correlated oxide $La_{1.5}Sr_{0.5}CoO_4$

A. T. Savici,[1] I. A. Zaliznyak,[1] G. D. Gu,[1] and R. Erwin[2]

[1]*DCMPMS, Brookhaven National Laboratory, Upton, New York 11973-5000*
[2]*NCNR, National Institute of Standards and Technology, Gaithersburg, Maryland 20899, USA*

(Dated: February 5, 2008)

We studied the nano-scale structure of the short-range incommensurate magnetic order in $La_{1.5}Sr_{0.5}CoO_4$ by elastic neutron scattering. We find that magnetic diffuse scattering is isotropic in the $a-b$ plane, in contrast with the naive expectation based on the popular stripe model. Indeed, charge segregation into lines favoring certain lattice direction(s) would facilitate linear stacking faults in an otherwise robust antiferromagnetism of un-doped material, leading to anisotropic disorder, with a characteristic symmetry pattern present in the neutron scattering data.

PACS numbers: 71.28+d, 75.40.Cx, 75.40.Gb, 75.50.Ee

I. INTRODUCTION

Ever since the advent of high-temperature superconductivity (HTSC) in cuprates, the physics of doped strongly correlated transition metal oxides remains at the forefront of condensed matter research.[1,2,3] In particular, there is a renewed interest in metal-insulator transitions associated with charge/orbital ordering in doped manganese and nickel oxides and in "colossal" magnetoresistance phenomena.[3,4,5] While macroscopic magnetic and transport properties of strongly correlated oxides respond to doping in many different and often fascinating ways, the appearance of structural and magnetic superlattices whose periods depend on the doping level is a common microscopic response shared by many oxides.[6,7,8,9,10,11,12,13,14,15]

Simultaneous incommensurate magnetic and charge ordering was probably first observed in a doped nickelate, $La_{2-x}Sr_xNiO_{4+y}$.[6] It gained prominence when a similar phenomenon was discovered in a $x \approx 1/8$ doped cuprate with an anomalously suppressed superconductivity.[7] It was proposed that a simple model of real-space static ordering of holes and spins, where doped charges segregate into lines separating magnetically ordered stripe domains, can explain all features observed by elastic neutron scattering. In conjunction with earlier theoretical predictions of such superstructures in the 2D Hubbard model, which is believed to describe the physics of HTSC cuprates,[16,17,18,19] striped phases gained broad popularity and became essentially a default model for describing incommensurate magnetic and charge superstructures in doped layered perovskite oxides $La_{2-x}Sr_xMO_4$ (M = Cu, Ni, Co, Mn).

There is a growing recognition, however, that physics of charge ordering in cuprates may differ significantly from that in well-insulating materials such as cobaltates and nickelates, where it can also be viewed as ordering of polarons driven by lattice elastic interactions.[20,21,22] In fact, it was argued theoretically that formation of superstructures whose period depends on the doping level, including stripes, is a natural response of the crystal lattice to local strain associated with doped charges and can be already explained by considering the system's elastic energy.[21] Experiments indicate this type of superlattices in layered manganates and cobaltates.[13,14,15]

In a superlattice, e.g. such as associated with polaron ordering, atomic positions and/or alignment of magnetic moments do not vary in the direction perpendicular to the propagation vector, presenting superlattice modulation as a periodic arrangement of lines of parallel spins and/or identical atomic displacements (Fig. 1). Hence, stripe superstructures resulting from one-dimensional electronic phase segregation and elas-

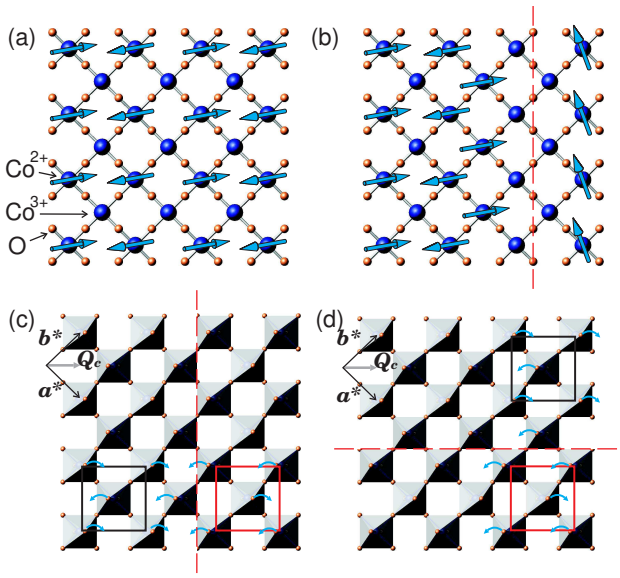

FIG. 1: (a) Checkerboard charge and spin order at half-doping. (b) Stacking fault giving rise to short-range correlation and magnetic incommensurability in $La_{1.5}Sr_{0.5}CoO_4$ in stripe picture. (c), (d) LTO superlattice of weakly doped cuprates. $\mathbf{a}^*$, $\mathbf{b}^*$ are reciprocal lattice vectors of the HTT phase, arrows show tilts of O octahedra. Stacking faults separating structural domains with opposite tilts (broken lines) running along "stripes" (perpendicular to Q_c), (c), and perpendicular to "stripes" (parallel to Q_c), (d), have the same energy, implying isotropic disorder.

tic/magnetic superlattices have similar appearance in real space. Accounting for domains, they also give rise to similarly positioned elastic peaks observable in scattering experiments. Hence, the question arises: is it possible to distinguish between the two cases? Here we show that for short-range superstructures this question can be answered by studying the nano-scale structure of disorder. By measuring the pattern of elastic neutron scattering, we find that short-range incommensurate magnetism in half-doped cobaltite $La_{1.5}Sr_{0.5}CoO_4$ does not originate from an intrinsically one-dimensional stripe charge order.

At half-doping, the system is naturally amenable to a checkerboard charge order (CO) where every other site in the $a-b$ plane of the high-temperature tetragonal (HTT) structure accommodates a hole, Fig. 1 (a). It is accompanied by a correlated harmonic modulation of atomic positions with propagation vector $Q_c = (1/2, 1/2)$ in the HTT reciprocal lattice, resulting in a superlattice with twice larger unit cell compared to the HTT phase where $a = b \approx 3.83$ Å. In stripe picture this type of CO can be viewed as an alternate stacking of diagonal charge stripes. The CO structural disorder results from faults in stripe stacking, Fig. 1 (b), and is one-dimensional (1D) in nature. The ordering of small polarons driven by lattice strain, on the other hand, is in essence similar to the cooperative tilt pattern of oxygen octahedra in the low-temperature orthorhombic (LTO) lattice, which relieves chemical pressure in weakly doped cuprates, Fig. 1(c,d). Stacking faults have no intrinsic 1D rigidity and result in randomly shaped domains and isotropic disorder.

Although $x = 0.5$ regime is inaccessible in cuprates, checkerboard CO was found for M = Ni, Co, Mn.[11,13,14,15] While there is no yet consensus on the cobaltate, ordering in Mn material is commonly viewed as a cooperative Jahn-Teller distortion, or CDW, driven mainly by lattice elastic energy,[13] while that in the nickelate is usually discussed in terms of stripes,[11] following the original proposition of Ref. 6. Although for different reasons, hole sites are effectively nonmagnetic both in cobaltite and nickelate; antiferromagnetic spin order (SO) on the remaining sites gives rise to a superlattice with four times the period of the original HTT lattice, Fig. 1(a). Experiments show that this spin order is usually short-ranged, most probably reflecting the short-range nature of charge/stripe superlattice. Then, it would be natural to expect that structure of these short-range nano-scale spin correlations reflects the structure of faults in the charge order, e. g. a disorder in the form of linear magnetic disclinations associated with stripe stacking faults, Fig. 1(b).

II. EXPERIMENTAL PROCEDURE

We studied a large single crystal of $La_{1.5}Sr_{0.5}CoO_4$ ($m \approx 11$ g) grown by the floating zone method. It has a nearly HTT structure with lattice parameters $a = b \approx 3.83$ Å and $c \approx 12.5$ Å at T = 10 K and was previously described in Ref. 15. Sample mosaic spread is $\eta \approx 20'$. Measurements were done in (h,k,0) and (h,h,l) reciprocal lattice zones using cold (SPINS) and thermal (BT9) neutron triple axis spectrometers, respectively, at NIST Center for Neutron Research. Monochromatic neutrons were obtained using (002) reflection from vertically focussing pyrolytic graphite (PG) crystals and analyzed using flat PG(002) analyzer crystals. On SPINS beam collimations were $\approx 37' - 80' - 80' - 240'$, from guide to detector, and neutron final energy was $E_f = 5$ meV. Beryllium filters both before and after the sample were used to remove the contamination from higher order reflections in PG. On BT9 we used $E_f = 14.7$ meV, collimations $\approx 40' - 40' - 40' - 100'$, and PG filters before and after the sample.

Color contour maps of the measured elastic scattering intensity are shown in Fig. 2 (a,b). Both in (h,k,0) (a) and (h,h,l) (b) zones the observed peaks are much broader than the calculated instrument resolution, which is illustrated by the FWHM ellipses. Peaks of magnetic origin are at $h, k \approx 0.25$ and 0.75, while those due to atomic displacement accompanying charge ordering are at h = k = 0.5. Checkerboard CO in $La_{1.5}Sr_{0.5}CoO_4$ sets in at about 825 K, while magnetic spin ordering appears only below abound 30 K.[15]

Selected scans around the magnetic peak position are presented in Figure 3. The lines show the result of the global fit of all data to the resolution corrected anisotropic cross section given by Eq. (5) for $D = 3$, which is discussed in detail in the next section.

Quantifying the nano-scale structure of short-range magnetic correlations experimentally so as to distinguish between various symmetries of magnetic domains requires accurate knowledge and deep understanding of the resolution effects present in neutron scattering measurements. In order to quantify the resolution function and accurately account for the resolution effects we measured elastic scattering intensity around (1,1,0) Bragg peak, in the (h,k,0) orientation. The data scaled down by a factor of 100 in order to roughly fit in the intensity range of magnetic scattering are shown in the upper right corner of the contour plot of Figure 2(a). It is immediately clear that magnetic peaks are much broader than nuclear lattice peak, whose width is governed entirely by the resolution and sample mosaics. A more detailed image of intensity around (1,1,0) nuclear Bragg peak is shown in Fig. 4 (a). Intensity scale enhances regions with smaller number of counts away from the peak.

Resolution of the triple axis neutron spectrometer is usually described using Cooper-Nathans formalism.[23] We show the result of such calculation for the (110) nuclear Bragg reflection in Fig. 4 (b). There is an obvious discrepancy between the calculation and the observed intensity shown in Fig. 4 (a), which has a pronounced tail along k-direction, resulting in an elliptical Bragg spot on the contour map. This shape can be explained by taking into account the sample size effects (our sample is a ≈ 5 cm long cylinder, which for scattering measurement in

the (h,k,0) zone is mounted roughly parallel to the scattering plane). In a very general way, this can be done by using the method devised by Popovici,[24] where sample is described in terms of a Gaussian density distribution. Instead, here we have explicitly included the sample size in the Cooper-Nathans calculation by averaging over the scattering angle between the incident and scattered neutron beams, which varies across the length of the sample. The result of such calculation gives very good fit of the measured (110) nuclear Bragg intensity, which is plotted in Fig. 4 (c). Sample mosaic was found to be 0.3°.

Mosaic structure of the (110) nuclear Bragg reflection in Fig. 4 (a) consists of a single peak, with no apparent indication of an orthorhombic lattice distortion.[25]

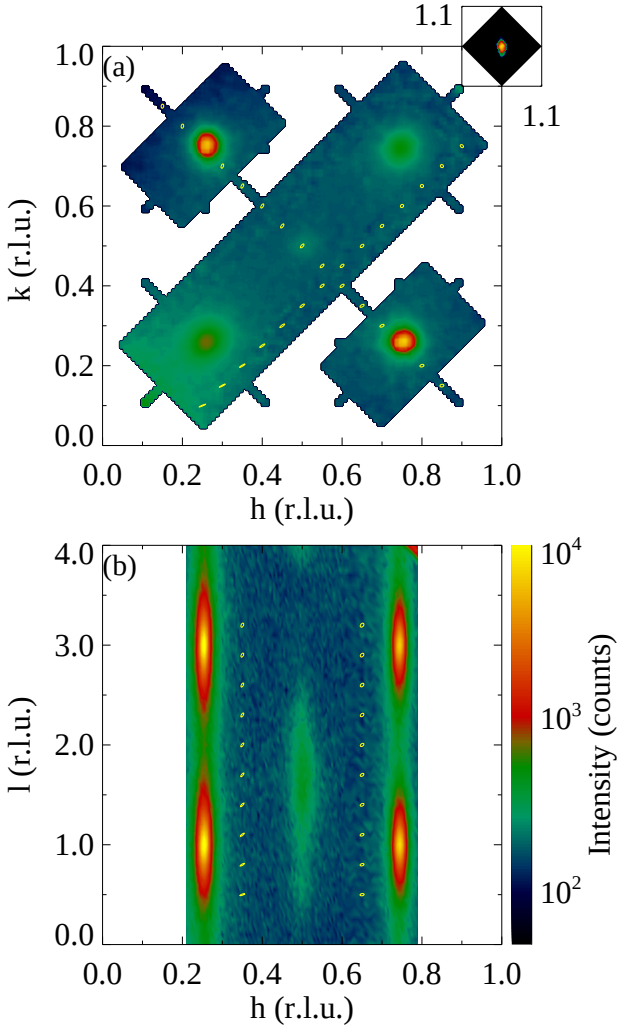

FIG. 2: Contour map of the measured neutron elastic scattering intensity in (h,k,0) (a) and (h,h,l) (b) zones at T = 3.5 K and 10 K, respectively. Ellipses show the calculated full width at half maximum (FWHM) instrument resolution.[23] Magnetic peaks are at $h, k \approx 0.25, 0.75$ r.l.u. Charge order scattering is seen at h = k = 0.5 r.l.u. Intensity in the map around (1,1,0) Bragg peak shown in the top right corner was scaled down by a factor of 100.

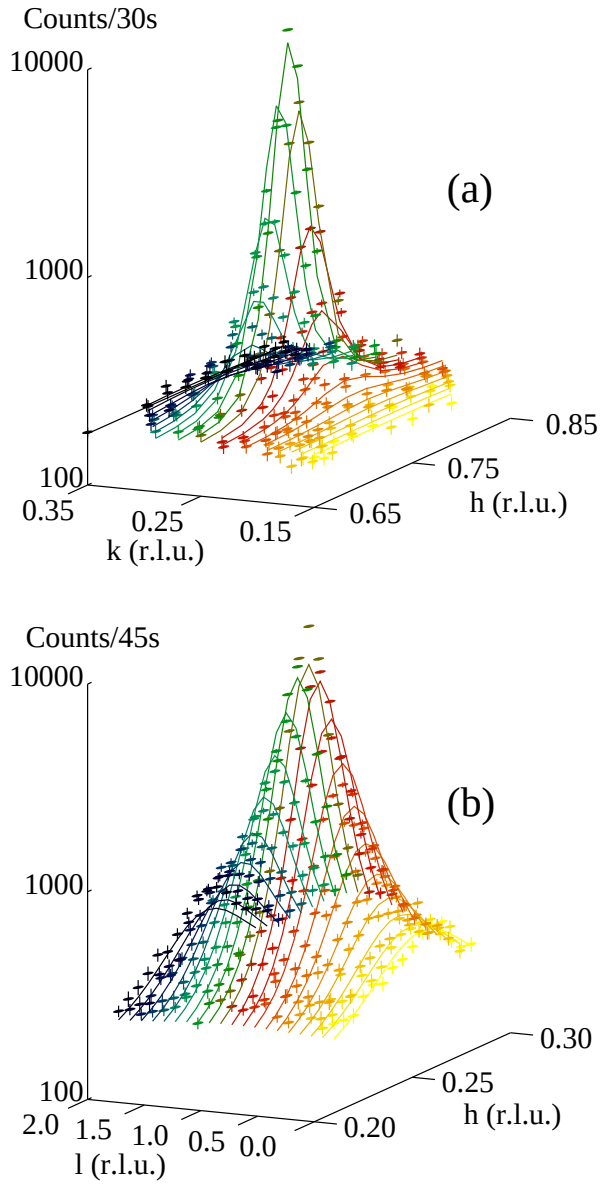

FIG. 3: Elastic neutron scattering from $La_{1.5}Sr_{0.5}CoO_4$. (a) (h,k,0) reciprocal lattice zone, (b) (h,h,l) zone. The lines show the global fit of the data to Eq. (5) describing coupled anisotropic 3D correlations.

Therefore, if present, any such distortion is not detectable within the accuracy of our measurement of nuclear Bragg reflections. However, we find a small, $\sim 0.6\%$ distortion from the analysis of magnetic scattering, which is described below.

III. ANALYSIS AND DISCUSSION

An appealing feature of stripe picture is that it provides a simple real-space model explaining both

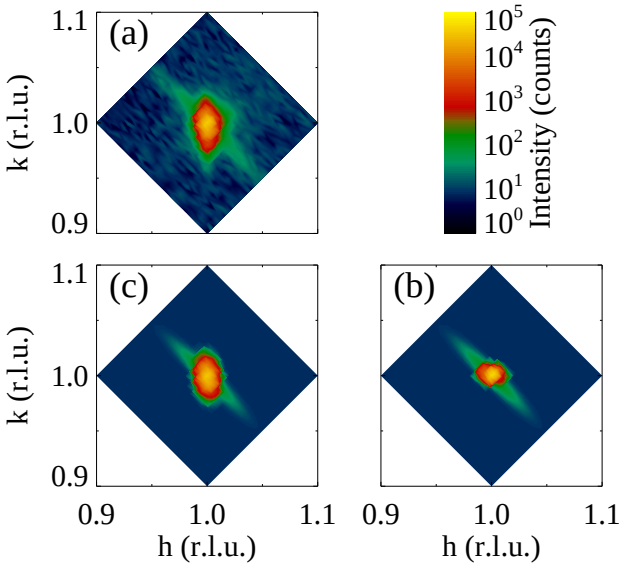

FIG. 4: Resolution and sample size effects for (1,1,0) Bragg reflection. (a) Contour map of the measured neutron scattering intensity in the (h,k,0) zone at T = 3.5 K. (b) Calculated intensity for the point-like sample, corresponding to the resolution-broadened delta function.[23] (c) Same as in (b), but with sample size effects included. Small extra intensity extended along a diagonal corresponds to a small ($\sim 0.3\%$) oriented powder component with angular distribution of $\approx 0.8^\circ$, much broader than sample mosaic spread $\eta \approx 0.3^\circ$.

temperature-dependent CO incommensurability in nickelates and short-range incommensurate magnetism in both Ni and Co materials.[11] In this picture they arise from discommensurations, or faults in the stacking pattern of 1D charge/spin stripes, favored by strong nearest-neighbor exchange coupling on the HTT square lattice, Fig. 1 (b). At half-doping such faults effectively reduce the average period of magnetic structure within the correlated domains in $a-b$ plane, consistent with slightly longer than (1/4,1/4) SO wave vector $Q_{\rm so} \approx (0.256, 0.256)$ in $La_{1.5}Sr_{0.5}CoO_4$.[15] It is also clear from the figure that discommensurations introduce linear disclinations parallel to stripes (coupling across two consecutive hole sites is weak and frustrated) and therefore truncate spin correlation range. This type of disorder has a specific imprint in the structure of diffuse elastic peaks measured in scattering experiment.[27,28,29,30,31]

Anisotropic short-range-ordered superlattices are well known in the physics of imperfect crystals and binary alloys, such as Cu_3Au.[27,28,29,30] Phase mismatches at the boundaries of antiphase domains and/or stacking faults introduce one-dimensional disorder in the direction perpendicular to the defect planes. A combination of several systems of such phase slips allowed in the crystal structure leads to a peculiar X-ray (and neutron) scattering pattern, with tails along certain lattice directions.[27,29]

Similar considerations can be extended to scattering by short-range magnetic structures where disorder results from un-correlated stacking faults (disclinations), such as shown in Fig. 1 (b).[32] The elastic magnetic neutron scattering cross section is given by

$$\frac{d\sigma(\mathbf{q})}{d\Omega} = N\left(\frac{r_m}{2\mu_B}\right)^2 \sum_j^N \mathrm{e}^{-i\mathbf{q}\cdot\mathbf{R}_j} \langle \mathbf{M}_0^\perp(-\mathbf{q}) \mathbf{M}_j^\perp(\mathbf{q})\rangle, \quad (1)$$

where $r_m \approx -5.39\cdot 10^{-13}$cm, μ_B is the Bohr's magneton, $\mathbf{M}_j^\perp(\mathbf{q})$ is the perpendicular to the wave vector $\mathbf{q}$ component of the Fourier-transform of the magnetization of atoms belonging to the lattice unit cell at a position $\mathbf{R}_j$, and the sum extends over all N unit cells of the crystal. In the presence of long-range magnetic order with wave vector $\mathbf{Q}$,

$$\langle \mathbf{M}_j(\mathbf{q})\rangle = \mathbf{m}(\mathbf{q})\mathrm{e}^{i\mathbf{Q}\cdot\mathbf{R}_j} + \mathbf{m}^*(\mathbf{q})\mathrm{e}^{-i\mathbf{Q}\cdot\mathbf{R}_j}, \quad (2)$$

where the order parameter $\mathbf{m}(\mathbf{q})$ includes Wannier function describing magnetic form factor of the unit cell. Fourier-transform in Eq. (1) is a sum of delta-functions offset by $\mathbf{Q}$ from reciprocal lattice points.

Un-correlated magnetic disclinations in the crystal can be accounted for by introducing additional random phase multipliers $e^{-i\phi_j}$ in the magnetization density (2). In view of its randomness, averaging over this phase factor can be decoupled in the correlation function in Eq. (1). Assuming self-averaging and Gaussian randomness, its statistical average is $\langle e^{-i\phi_j}\rangle = e^{-\langle\phi_j^2\rangle/2}$ (Bloch identity) and the scattering cross-section is

$$\frac{d\sigma(\mathbf{q})}{d\Omega} = Nr_m^2 \left|\frac{\mathbf{m}^\perp(\mathbf{q})}{2\mu_B}\right|^2 \sum_j^N \mathrm{e}^{-i\mathbf{q}\cdot\mathbf{R}_j - \frac{1}{2}\langle\phi_j^2\rangle}. \quad (3)$$

In the case of planar (linear in 2D) disclinations perpendicular to principal lattice directions such as expected from stripes, the accumulated mean-square phase mismatch can be described by independent random walks along these directions. Then, $\langle\phi_j^2\rangle/2 = \sum_\alpha |n_{j,\alpha}|/\xi_\alpha$, where $n_{j,\alpha}$ label lattice sites, $\mathbf{R}_j = \sum_\alpha n_{j,\alpha}\mathbf{a}_\alpha$, and ξ_α are correlation lengths in appropriate units ($\alpha = x, y, z$). Substituting this into Eq. (1), one obtains cross-section in the form of a product of 1D lattice-Lorentzians (LL),

$$\tilde{L}_{\xi_\alpha}(q_\alpha) \equiv \frac{\sinh\xi_\alpha^{-1}}{\cosh\xi_\alpha^{-1} - \cos(q_\alpha \pm Q_\alpha)}, \quad (4)$$

along principal crystallographic directions (Eq. (4) is a sum of Lorentzians placed periodically in reciprocal lattice). Factorized cross-section is a consequence of the 1D nature of disorder generated by system of linear/planar phase slips. It retains the orientational symmetry of these defects in the crystal lattice.

If, perhaps upon appropriate re-scaling of co-ordinates, the disorder is isotropic, such as introduced for example by the domain structure in the random field Ising model (RFIM),[33] phase slips depend only on $|\mathbf{R}_j|$ and $\langle\phi_j^2\rangle/2 = \frac{|\mathbf{n}_j|}{\xi}$. While the lattice sum can not be easily evaluated,

TABLE I: Scattering functions for different structure of the nano-scale disorder on a 3D lattice (assuming large ξ_α).

type of disorder	scattering cross section
1D×1D×1D	$(1+q_1^2\xi_1^2)^{-1}(1+q_2^2\xi_2^2)^{-1}(1+q_3^2\xi_3^2)^{-1}$
2D×1D	$(1+q_1^2\xi_1^2+q_2^2\xi_2^2)^{-1.5}(1+q_3^2\xi_3^2)^{-1}$
3D	$(1+q_1^2\xi_1^2+q_2^2\xi_2^2+q_3^2\xi_3^2)^{-2}$

it can be rewritten as an integral which is repeated periodically in reciprocal lattice and summed to restore the lattice translational symmetry. For a D-dimensional lattice ($D = 1, 2, 3$), the result is a generalized-lattice-Lorentzian function,

$$\sum_{\boldsymbol{\tau}} \left(1 + \sum_{\alpha=1}^{D} (q_\alpha \pm Q_\alpha + \tau_\alpha)^2 \xi_\alpha^2\right)^{-\frac{D+1}{2}}, \qquad (5)$$

where ξ_α are the original un-rescaled correlation lengths and $\boldsymbol{\tau}$ are reciprocal lattice vectors. Cross-section of the form given by Eq. 5 was observed in neutron scattering experiments in two- and three-dimensional random field Ising ferro- and antiferro-magnets, in particular in $Rb_2Co_{0.7}Mg_{0.3}F_4$ and $Co_{0.35}Zn_{0.65}F_2$.[34,35]

Scattering functions for different combinations of disorder described by Eqs. (4) and (5) on a 3D lattice are summarized in Table I. A fully factorized (product of LL in all 3 directions) 1D×1D×1D cross-section can be expected in stripe picture for $La_{1.5}Sr_{0.5}CoO_4$. Indeed, discommensurations destroy magnetic correlation perpendicular to stripes without seriously affecting order along them. Similarly, the inter-plane correlation is destroyed by faults in plane stacking. Resulting diffuse scattering has diamond-like shape reminiscent of a superposition of quasi-1D "rods" of scattering extended perpendicular to stripes and/or planes, such as shown in Fig. 5(a). Cross-section corresponding to anisotropic 3D domains given by a lattice-Lorentzian-squared is shown in Fig. 5(b)

Whether the disorder-generating defects are independent linear/planar disclinations or not (i. e. independent of how the cross-section is factorized and which of the models listed in Table I is appropriate), one expects an in-plane anisotropy between the correlation length along and perpendicular to stripe direction within the stripe model.[26] Hence, within this model we expect two weak contributions to magnetic scattering in our sample, at the diagonal positions h = k ≈ 1/4, 3/4 in the (h,k,0) zone of the tetragonal unit cell, which are extended along this diagonal, indicating shorter correlations perpendicular to stripes. Their intensity is weak because they are just tails of magnetic peaks at (1/4,1/4,1) and (3/4,3/4,1) resulting from finite correlation length (peak width) along the c axis. The strong signal, which is present in our data at (1/4,3/4,0) and (3/4,1/4,0), arises from twin magnetic domains in the sample, and thus its intensity pattern is rotated by 90°. Overall, all peaks should exhibit C_2 symmetry and contributions from twin domains should be rotated 90° with respect to each other.

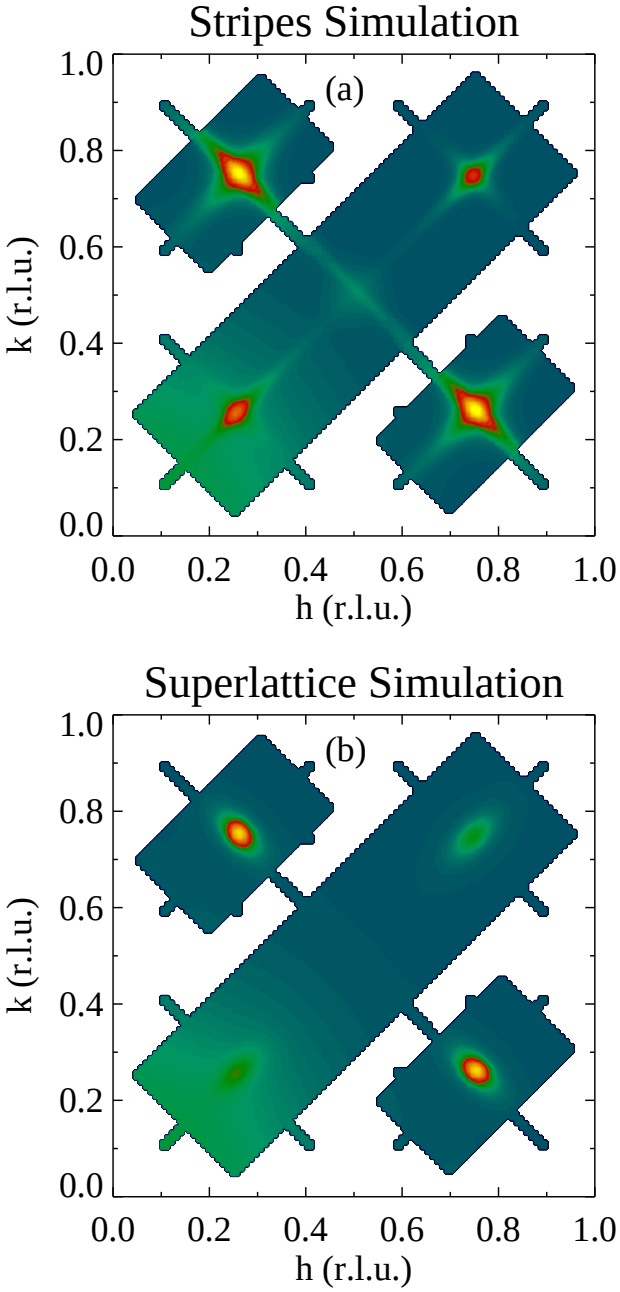

FIG. 5: Simulated magnetic scattering intensity for $La_{1.5}Sr_{0.5}CoO_4$ in the (h,k,0) reciprocal lattice zone with anisotropic correlation lengths in the a-b plane $\xi_{1,1,0} = 9.2$ and $\xi_{1,-1,0} = 18.4$ LTO (HTT diagonal) lattice units (l.u.). 2:1 ratio of the correlation lengths corresponds to findings of Ref. 26. (a) factorized 1D lattice Lorentzian cross-section (b) Lorentzian-squared corresponding to anisotropic 3D disorder.

In Figure 5 we show simulated magnetic scattering intensity for our sample arising from anisotropic short-range magnetic correlations expected in the stripe model with correlation length ratio 2:1, chosen to compare with the data of Ref. 26. Fig 5 (a) shows simulated neutron scattering data for the factorized-lattice-

Lorentzian cross-section, while scattering corresponding to the lattice-Lorentzian-squared from anisotropic 3D correlations is presented in Fig 5 (b). Equal contributions from both twin domains were assumed.

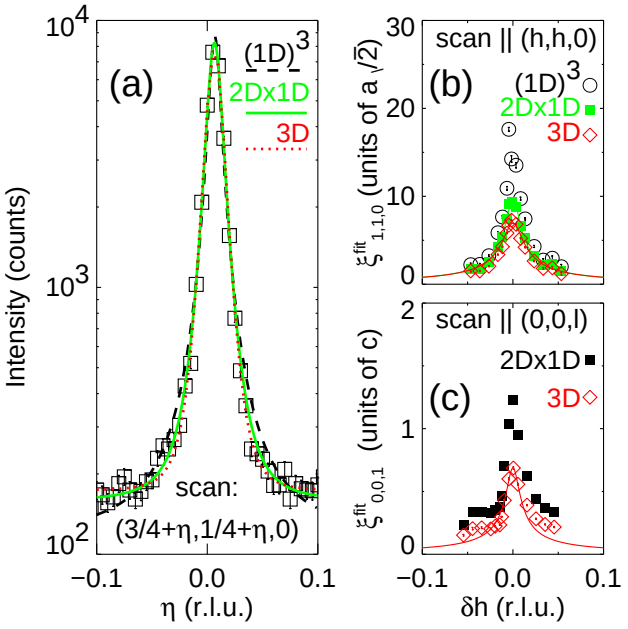

FIG. 6: (a) Typical scan through magnetic peak with fits to cross-sections for completely independent linear disclinations [(1D)^3], isotropic disorder in $a-b$ plane with stacking faults along c (2Dx1D), or disorder coupled in all 3 directions (3D). (b) and (c) "correlation length" for scans offset by δq from the magnetic peak position, $\mathbf{Q} \approx (0.744{+}\delta h, 0.256{-}\delta h, 0)$ for (b) and $\mathbf{Q} \approx (0.256{+}\delta h, 0.256{+}\delta h, 1)$ for (c). The solid/dashed lines are single-parameter fits to Eq. 6, $\delta q = \delta h\sqrt{2}$.

From comparing Fig. 2 (a, b) and Fig. 5 (a, b) it is already clear that short-range magnetic order in $La_{1.5}Sr_{0.5}CoO_4$ is neither anisotropic in the $a-b$ plane, nor it is described by independent one-dimensional magnetic disclinations associated with stripes running along diagonals of the HTT unit cell, Fig. 1 (b). It is rather consistent with anisotropic short-range 3D superlattice model with equal correlation lengths in the $a-b$ plane. This can be further quantified by fitting to Eq. (5) 1D scans made at different off-sets δq from the magnetic peak position along the diagonal of the HTT unit cell, Fig. 6 (a). "Correlation lengths" obtained from such fits of scans along (h,h,0) and (0,0,l) directions are shown in Fig. 6. For now, we neglect the instrumental resolution effects which are small compared to much larger width of magnetic/charge order peaks. In this case, for the factorized LL scattering cross-section so determined ξ_α should be independent of δq, while for D = 2,3,

$$\xi_\alpha^{fit} = \xi_\alpha / \sqrt{1 + \sum_{\beta\neq\alpha} (\delta q_\beta \xi_\beta)^2}, \qquad (6)$$

where ξ_α is magnetic correlation length in the corresponding direction. Fits shown in Fig. 6 (b) and (c) using Equation 6 yield $\xi^{3D}_{1,1,0}$=7.0 and $\xi^{2D\times1D}_{1,1,0}$=9.6 (HTT diagonal) lattice units, and $\xi^{3D}_{0,0,1}$=0.68 l.u. Note, that these values are obtained neglecting the resolution corrections, and thus represent lower limits for the corresponding correlation length.

While different fits to 1D scan through magnetic peak shown in Fig. 6 (a) can be hardly distinguished, variation of the fitted correlation length $\xi^{fit}_{1,1,0}$ with off-set from the peak position shown in Fig. 6 (b) is clearly inconsistent with the factorized scattering cross-section expected for independent disclinations associated with stripes in the $a-b$ plane. Moreover, variation of ξ^{fit}_c obtained from measurements around (1/4,1/4,1) in the (h,h,l) zone shown in Fig. 6 (c) rules out factorization into a 2D dependence in the $a-b$ plane and a 1D dependence along c-axis, such as arises from independent planar stacking faults. Therefore, our results are best described by Eq. (5) with D=3 and anisotropic correlation lengths, indicating disorder typical of an anisotropic 3D random field Ising model.[33] This is further confirmed quantitatively by fitting the entire data set to resolution corrected cross sections from Table I. Such fits yield χ^2 per degree of freedom values of 6.4 (3D), 10.3 (2D×1D) and 13.6 [(1D)^3]. For the 3D case (fits are shown in Fig. 3 and Fig. 7 (e, f)) we obtain correlation lengths $\xi_{1,1,0} = \xi_{1,-1,0}$= 9.4 LTO (HTT diagonal) lattice units (50.9 Å) and ξ_c= 0.58 l.u. (7.25 Å). For 2D × 1D case, $\xi_{1,1,0} = \xi_{1,-1,0}$= 10.2 l.u. (55.2 Å), ξ_c= 0.9 l.u. (11.3 Å) and for 1Dx1Dx1D case, $\xi_{1,1,0} = \xi_{1,-1,0}$= 13.3 l.u. (72.1 Å), ξ_c= 1.1 l.u. (13.8 Å). The latter compare well with the previous results of Ref. 15, although now it is clear from our present data that a factorized cross-section is not an appropriate model for magnetic scattering in $La_{1.5}Sr_{0.5}CoO_4$. Color contour plots of the calculated intensities corresponding to the above fitting results are shown in Figure 7.

Finally, we also found that magnetic scattering pattern in (hk0) zone allows us to refine small orthorhombic distortion of the crystal lattice of about 0.6% in the $a-b$ plane ($a/b \approx 1.006$).

IV. SUMMARY AND CONCLUSIONS

In summary, incommensurate magnetic and charge superstructures observed in hole-doped cuprates, nickelates and cobaltates $La_{2-x}Sr_xMO_4$ (M = Cu, Ni, Co, Mn) are often described in terms of discommensurations in the quasi-regular stacking of charge lines separating antiferromagnetically ordered stripe domains. Existence of such faults in stripe stacking has two essential consequences. First, it renders the super-lattice incommensurability, which can explain the temperature-dependent incommensurate magnetism observed in hole-doped nickelates with $0.25 \lesssim x \lesssim 0.5$.[11,12] Secondly, stacking faults truncate the super-lattice coherence, resulting in a short-range glassy superstructure, which manifests itself in ex-

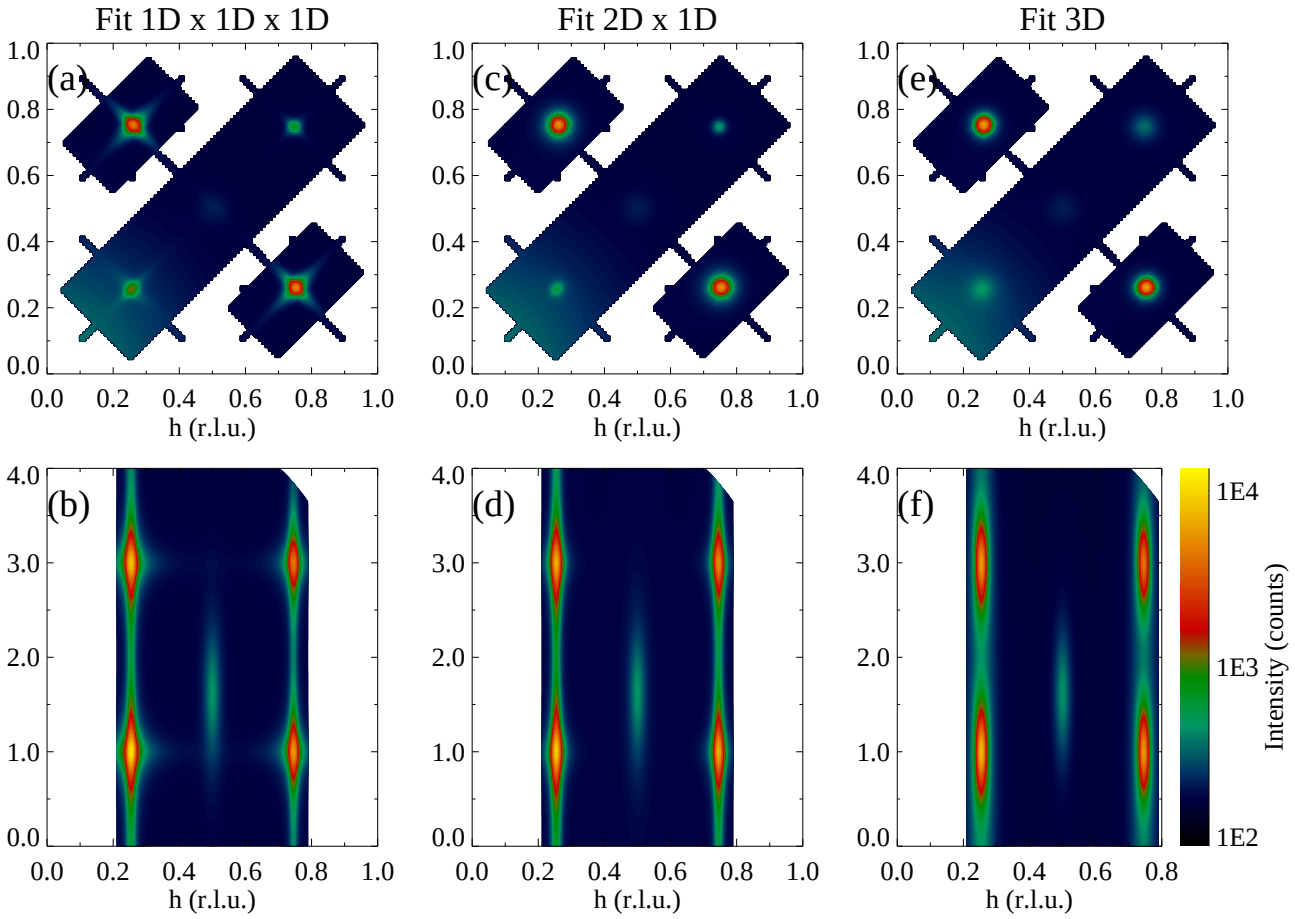

FIG. 7: Fit results of neutron scattering intensity in (h,k,0) (a),(c),(e) and (h,h,l) (b),(d),(f) zones at T=3.5K and 10K. 1D×1D×1D correlation (stripe-like) are in (a) and (b).(c) and (d) show results for 2D×1D correlations. (e) and (f)Fitted intensity patterns for coupled isotropic correlations (superlattice)

periment by finite-width, diffuse peaks of elastic scattering in place of Bragg reflections.

Experimental studies of short-range magnetic and/or charge scattering such as presented in this paper provide an important tool for investigating spin- and charge-ordered phases and testing various flavors of stripe models. Our results present strong evidence that stripe-type superstructure is not at the origin of incommensurate short-range magnetism in the half-doped cobaltate $La_{1.5}Sr_{0.5}CoO_4$. This is not completely unexpected, as charge order in this material occurs independently of magnetic order, in a well-insulating state and at much higher temperature.[15] It is mainly driven by lattice electrostatics and local spin entropy competing with the crystal field splitting of Co ion's energy levels. Magnetic incommensurability in this picture can result from an inhomogeneous exchange modulation induced by CO.[36] The rigidity of quasi-1D charge-stripe segregation, on the other hand, is rendered by the kinetic energy of charge hopping,[7,16,17] which seems insignificant in our case. Our analysis can be applied to investigating the relevance of kinetic energy driven segregation of doped charges into stripes in cuprates and for "diagonal stripe" CO in other insulating $La_{2-x}Sr_xMO_4$ oxides. Such studies of "stripe-ordered" nickelates and cuprates are currently under way.

Acknowledgments

We thank NIST Center for Neutron Research for hospitality and J. Tranquada and M. Hücker for discussions. This work was performed under Contract DE--AC02-98CH10886, Division of Material Sciences, US Department of Energy, and utilized facilities supported in part by the National Science Foundation under Agreement DMR-0454672.

[1] P. A. Lee, N. Nagaosa, X.-G. Wen, Rev. Mod. Phys. **78**, 17 (2006).

[2] J. Orenstein, A. J. Millis, Science **288**, 468 (2000).

[3] Y. Tokura, Physics Today **7**, 50 (2003).
[4] Y. Tokura, N. Nagaosa, Science **288**, 462 (2000).
[5] M. Imada, A. Fujimori, Y. Tokura, Rev. Mod. Phys. **70**, 1039 (1998).
[6] J. M. Tranquada, D. J. Buttrey, V. Sachan, J. E. Lorenzo, Phys. Rev. Lett. **73**, 1003 (1994).
[7] J. M. Tranquada, B. J. Sternlieb, J. D. Axe, Y. Nakamura, S. Uchida, Nature **375**, 561 (1995); J. M. Tranquada, J. D. Axe, N. Ichikawa, Y. Nakamura, S. Uchida, B. Nachumi, Phys. Rev. B **54**, 7489 (1996).
[8] B. O. Wells, Y. S. Lee, M. A. Kastner, R. J. Christianson, R. J. Birgeneau, Y. Yamada, Y. Endoh, G. Shirane, Science **277**, 1067 (1997).
[9] C. H. Chen,S-W. Cheong, A. S. Cooper, Phys. Rev. Lett. **71**, 2461 (1993).
[10] H. Yoshizawa, T. Kakeshita, R. Kajimoto, T. Tanabe, T. Katsufuji, Y. Tokura, Phys. Rev. B **61**, R854 (2000).
[11] R. Kajimoto, T. Kakeshita, H. Yoshizawa, T. Tanabe, T. Katsufuji, Y. Tokura, Phys. Rev. B **64**, 144432 (2001); R. Kajimoto, K. Ishizaka, H. Yoshizawa, Y. Tokura, Phys. Rev. B **67**, 014511 (2003).
[12] K. Ishizaka, Y. Taguchi, R. Kajimoto, H. Yoshizawa, Y. Tokura, Phys. Rev. B **67**, 184418 (2003); K. Ishizaka, T. Arima, Y. Murakami, R. Kajimoto, H. Yoshizawa, N. Nagaosa, Y. Tokura, Phys. Rev. Lett. **92**, 196404 (2004).
[13] S. Larochelle, A. Mehta, N. Kaneko, P. K. Mang, A. F. Panchula, L. Zhou, J. Arthur, M. Greven Phys. Rev. Lett. **87**, 095502 (2001); S. Larochelle, A. Mehta, L. Lu, P. K. Mang, O. P. Vajk, N. Kaneko, J. W. Lynn, L. Zhou, M. Greven Phys. Rev. B 71, 024435 (2005).
[14] N. Sakiyama,I. A. Zaliznyak, S.-H. Lee, Y. Mitsui, H. Yoshizawa, unpublished.
[15] I. A. Zaliznyak, J. M. Tranquada, G. Gu, R. W. Erwin, Y. Moritomo, J. Appl. Phys. **95**, 7369 (2004).
[16] J. Zaanen, O. Gunnarsson, Phys. Rev. B **40**, 7391 (1989).
[17] V. J. Emery, S. A. Kivelson, Physica C **209**, 597 (1993).
[18] K. Machida, Physica C **158**, 192 (1989).
[19] M. Kato, K. Machida, H. Nakanishi, M. Fujita, J. Phys. Soc. Jpn., **59**, 1047 (1990).
[20] J. Zaanen, P. B. Littlewood, Phys. Rev. B **50**, 7222 (1994).
[21] D. I. Khomskii, K. I. Kugel, Europhys. Lett., **55**, 208 (2001).
[22] E. Collart, A. Shukla, J.-P. Rueff, P. Leininger, H. Ishii, I. Jarrige, Y. Q. Cai, S.-W. Cheong, G. Dhalenne, Phys. Rev. Lett. **96**, 157004 (2006).
[23] M. J. Cooper, R. Nathans, Acta Cryst. **23**, 357, (1967); S. A. Werner, R. Pynn, J. Appl.Phys. **42**,4736, (1971); N. J. Chesser, J. D. Axe, Acta Cryst. **A29**,160,(1972) .
[24] M. Popovici, Acta Cryst. **A31**, 507 (1975).
[25] T. Matsuura, J. Tabwchi, J. Mizusaki, S. Yamauchi, K. Fueki, J. Phys. Chem. Solids **49**, 1403, (1988).
[26] C-H. Du, M. E. Ghazi, Y. Su, I. Pape, P. D. Hatton, S. D. Brown, W. G. Stirling,M. J. Cooper,S-W. Cheong, Phys. Rev. Lett. **84**, 3911(2000).
[27] J. M. Cowley, J. Appl. Phys. **21**, 24 (1950).
[28] A. J. C. Wilson, Proc. Roy. Soc. **A180**, 277 (1942); *ibid.* **A181**, 360 (1943).
[29] B. E. Warren, *X-ray Diffraction* (Dover Publications, Inc., New York, 1990).
[30] M. A. Krivoglaz, *X-ray and Neutron Diffraction in Non-ideal Crystals* (Springer, New York, 1996).
[31] Y. Chen, W. Bao, Y. Qiu, J. E. Lorenzo, J. L. Sarrao, D. L. Ho, M. Y. Lin, Phys. Rev. B 72, 184401 (2005).
[32] I. A. Zaliznyak and S.-H. Lee, in *Modern Techniques for Characterizing Magnetic Materials*, Ed. Y. Zhu (Springer, New York, 2005).
[33] O. Zachar, I. Zaliznyak, Phys. Rev. Lett. **91**, 036401 (2003).
[34] R. J. Birgeneau, H. Yoshizawa, R. A. Cowley, G. Shirane, H. Ikeda, Phys. Rev. B **28**, 1438 (1983).
[35] M. Hagen, R. A. Cowley, S. K. Satija, H. Yoshizawa, G. Shirane, R. J. Birgeneau, H. J. Guggenheim, Phys. Rev. B **28**, 2602 (1983)
[36] I. A. Zaliznyak, Phys. Rev. B **68**, 134451 (2003).